Turkish J. Eng. Env. Sci.
30 (2006) , 135 – 143.

Simulation of Flameless Combustion of Natural Gas in a Laboratory Scale Furnace

Sébastien MURER, Barbara PESENTI and Paul LYBAERT
Thermal Engineering & Combustion Unit, Faculté Polytechnique de Mons,
Rue de l'Epargne, 56, B-7000, Mons, BELGIUM
e-mail: Sebastien.murer@fpms.ac.be

Received 01.06.2006

Abstract

The purpose of this study is to characterise the flameless combustion of natural gas, experimentally, and by CFD modelling with FLUENT. Measurements performed in a laboratory scale furnace are used as boundary conditions and validation data for the various models tested. Turbulence and combustion are respectively modelled with the standard k-ε model and the Eddy-Dissipation model, combined with the Finite Rate model. Experimentally and numerically, the furnace presents 2 regimes of combustion according to the chamber temperature. The first regime is called the "near-lifted flame" regime; it happens with high furnace temperatures, when the kinetics do not limit the reaction. In that mode, there are 2 main reaction zones separated by the furnace axis. The second regime is called the "far-lifted flame" regime; it appears when the furnace temperature level is lower and the Arrhenius limitation slows down the reaction rate. In that case, the combustion zone is wider and farther from the base of the chamber. The present paper compares the measured and computed shapes of the reaction zone.

Key words: Flameless combustion, Mild combustion, Numerical simulation, Diluted combustion.

Introduction

Combustion air preheating by flue gas heat recuperation is a well-known procedure for saving fuel. To abate the high NOx emissions occurring in high temperature air furnaces, the use of diluted combustion, also called "Mild Combustion" or "Flameless oxidation" in the literature, is very effective (Wünning and Wünning, 1997; Hasegawa and Tanaka, 1998). In the present work, the influence of furnace temperature and operating excess air on the flameless combustion of natural gas with highly preheated air is studied with CFD techniques and validated with experimental data measured in a laboratory scale furnace.

Experimental Set-Up

Figure 1a shows the experimental high temperature air combustion set-up used in this study. This set-up is described more precisely in the paper by Murer et al. (2005).

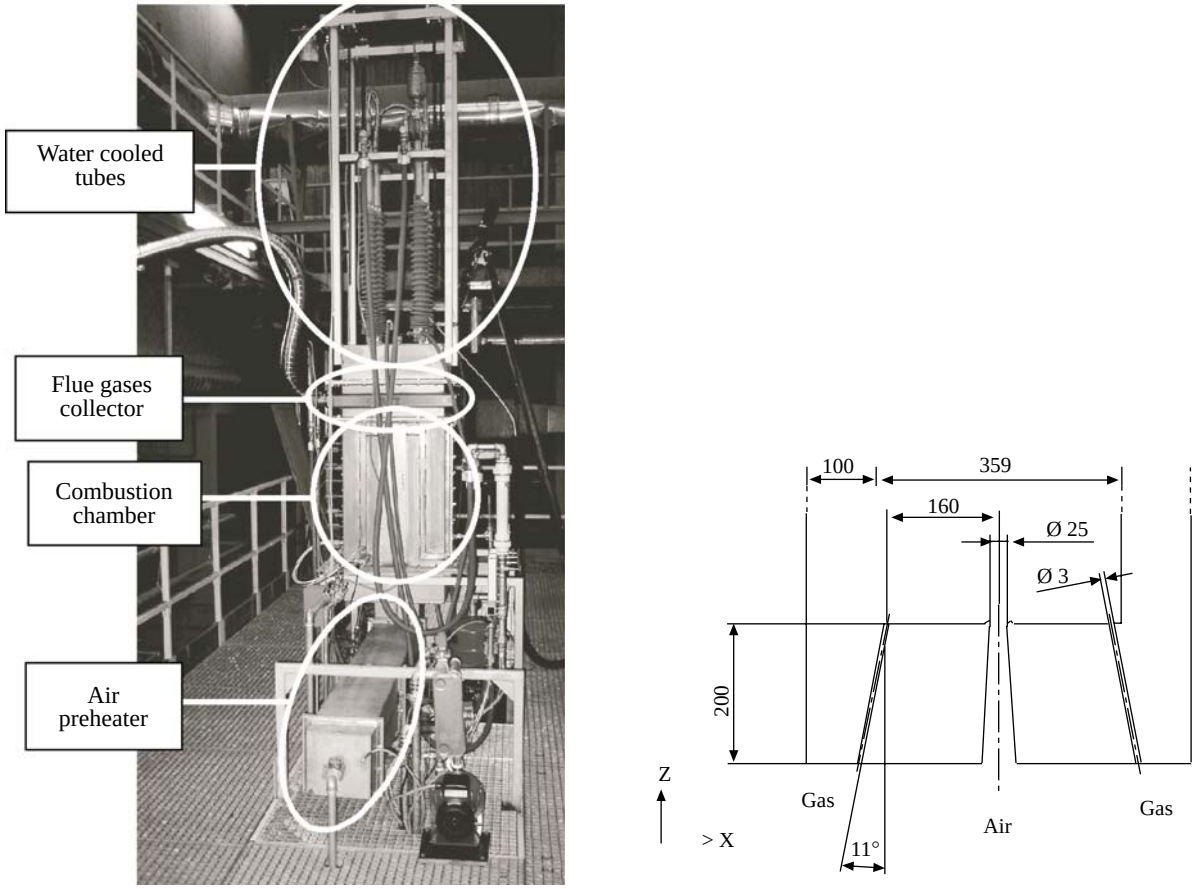

a) Pilot furnace b) Injectors scheme

Figure 1. Experimental set-up.

The combustion air can be preheated up to 1000 °C by an electrical heater. The air is then injected into the chamber through a 25 mm diameter nozzle (Figure 1b). Natural gas (88.7% CH_4) is introduced through 2 inclined injectors 3 mm in diameter. The furnace temperature is adjusted by varying the immersion depth of 4 water-cooled bayonet tubes. The burner configuration and the high inlet velocities generate the flameless combustion mode.

The following data are measured:

– Inlet (air and gas) temperatures and flow rates.

– Wall temperature profile (8 thermocouples along a vertical axis).

– Outlet gas temperature (suction thermocouple probe in the chimney).

– Flue gas composition (gas sampling by cooled probe at the furnace outlet).

Moreover, the combustion chamber is equipped with a vertical quartz window in order to perform flame imaging. An intensified CCD camera equipped with a narrow band pass filter was used to record UV self-emission of OH radicals. The reaction zone is characterised by analysis of the OH emission maps. The influence of the furnace inlet excess air ratio and furnace temperature on flame emission and furnace wall temperature profiles were investigated. The complete set of measured data has been reported in a previous work (Murer et al., 2005). An example of OH chemiluminescence images is shown in Figure 2, which represents the average of 50 instantaneous images. From these maps, the evolution of OH emission intensity was extracted on one vertical profile including the maximum intensity value of the picture (Figure 3). The resulting profiles are used for comparison with CFD results (see the section "Reaction zone volume and position").

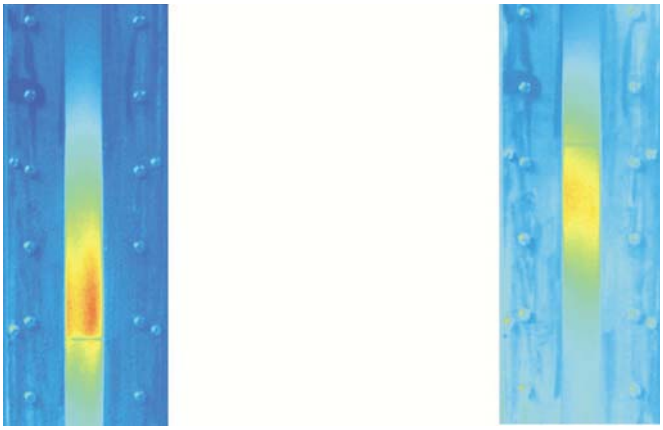

a) E = 10% – T_f = 1162 °C b) E = 10% – T_f = 1106 °C

Figure 2. UV imaging (50 pictures average). Φ_g = 30 kW, T_a = 1000 °C.

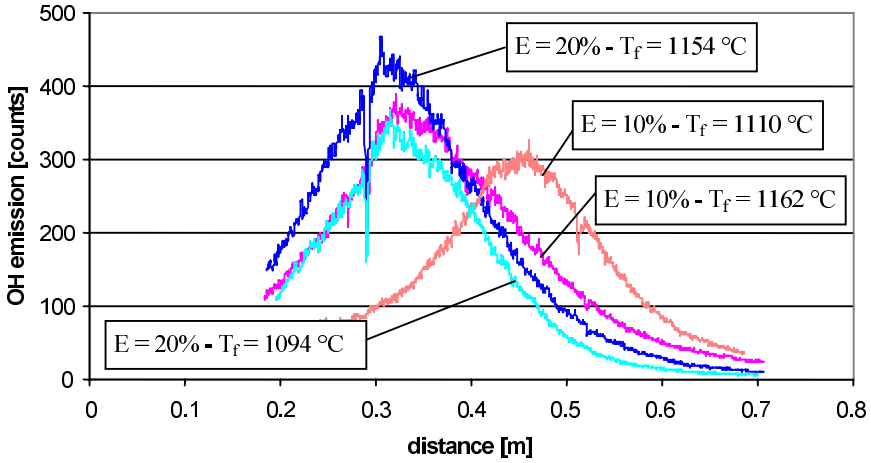

Figure 3. OH emission (Φ_g = 30 kW – T_a = 1000 °C).

CFD Modelling

CFD modelling of the test furnace was performed with version 6.1 of the FLUENT code.

Mesh

Thanks to symmetry, only a quarter of the furnace was modelled. Figure 4 shows the unstructured mesh used in the cross-section of the furnace. The 3-D mesh has been extruded from this 2-D mesh in the z-direction. Three different meshes were built, corresponding to the 3 immersion depths of the cooling tubes (0.3 m, 0.5 m, and 0.7 m). For example, the mesh built for an immersion of 0.5 m contains 241,005 hexahedral elements.

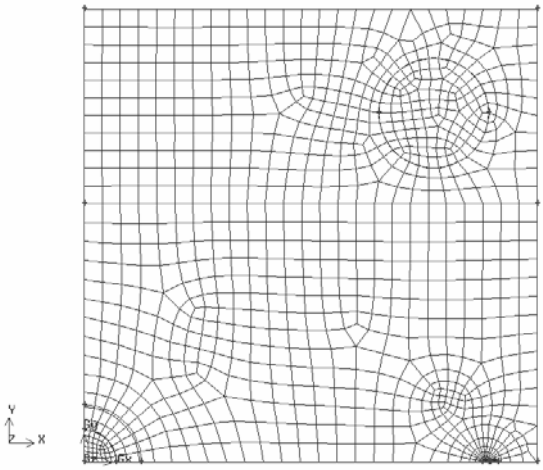

Figure 4. Cross-section of the mesh.

Model parameters and boundary conditions

Turbulence, combustion, and radiative transfer models were selected according to previous work (Murer et al., 2005). Regarding the very small differences resulting in the velocity and scalar fields computed by using the detailed Reynolds Stress Model compared to the standard k-ε model, turbulence was modelled in the present work using Launder and Spalding's standard k-ε model, with standard wall functions. The combustion reaction rates are computed as the minimum value of a mixing rate governed by the large eddy mixing time scale ("Eddy Dissipation Model" in Fluent 6.1) and an Arrhenius rate, governed by chemical kinetics ("Finite Rate Model" in Fluent 6.1). The chemical reaction mechanism is simulated by a 2-step reaction scheme with CO as the intermediate species and methane oxidation kinetic parameters from Westbrook and Dryer (1981).

Air and gas injection temperatures are imposed as measured and inlet velocities are computed from measured flow rates. Heat transfer at furnace walls and cooling tubes is imposed by choosing the walls' thermal conductivities and external temperatures. The walls' conductivities are chosen to adjust the computed heat losses to the corresponding experimental heat balance values (see Table). The furnace wall heat losses include the heat conducted through the insulation layer and the heat radiated through the visualisation window, which is not represented in the furnace model. The emissivity is chosen, respectively, at $\varepsilon = 0.3$ for the inner wall and at $\varepsilon = 0.5$ for the tubes.

The total fuel heating rate (Φ_g) and the air temperature (T_a) are constant at 30 kW and 1000 °C, respectively. The influence of excess air ratio (E) and furnace temperature has been investigated through modelling and the corresponding operating and boundary conditions are listed in Table. The inlet gas velocity is constant at 65 m/s; the air velocity is 76 m/s (E = 10%) or 83 m/s (E = 20%). The Table also compares measured flue gases outlet temperatures with the values computed with the same tube immersion depth. The discrepancies between computed and measured furnace temperatures indicate that the model boundary conditions still have to be adjusted to better reproduce furnace temperature conditions.

Results

Reaction zone volume and position

Characterisation of the reaction zone is deduced from the computed fields of temperature, CO mole fraction, and local heat release (computed from local reaction rates). Figures 5-8 show the fields computed for conditions 3-6, which are shown in Table.

On these maps, 2 significantly different combustion regimes can be observed. In Figures 5 and 6, the reaction begins in the vicinity of the gas injection and heat is completely released in the lower half of the furnace. The reaction zone is split into 2 regions symmetrically located on each side of the furnace axis.

Figures 5 and 6 show that the reaction can also occur in the recirculation zone enclosed between the gas jet and the furnace wall.

In Figures 7 and 8, the reaction begins farther downstream and heat is released in a larger volume. The 2 reaction zones become one unique, wider zone, and the temperature field in the furnace is more homogeneous.

Table. Operating conditions (Φ_g = 30 kW – T_a = 1000 °C).

	E	**Imm**	**Outlet temp. [°C]**		**Tube losses [kW]**		**Wall losses [kW]**	
	[%]	[m]	Exp	CFD	Exp	CFD	Exp	CFD
1	10	0.3	1213	1153	17.0	17.4	7.8	6.4
2	20	0.3	1198	1148	16.8	17.3	7.8	6.4
3	10	0.5	1131	1061	21.1	21.9	4.9	5.5
4	20	0.5	1120	1056	20.6	21.9	5.4	5.5
5	10	0.7		952		21.9		4.6
6	20	0.7		951		22.2		4.6

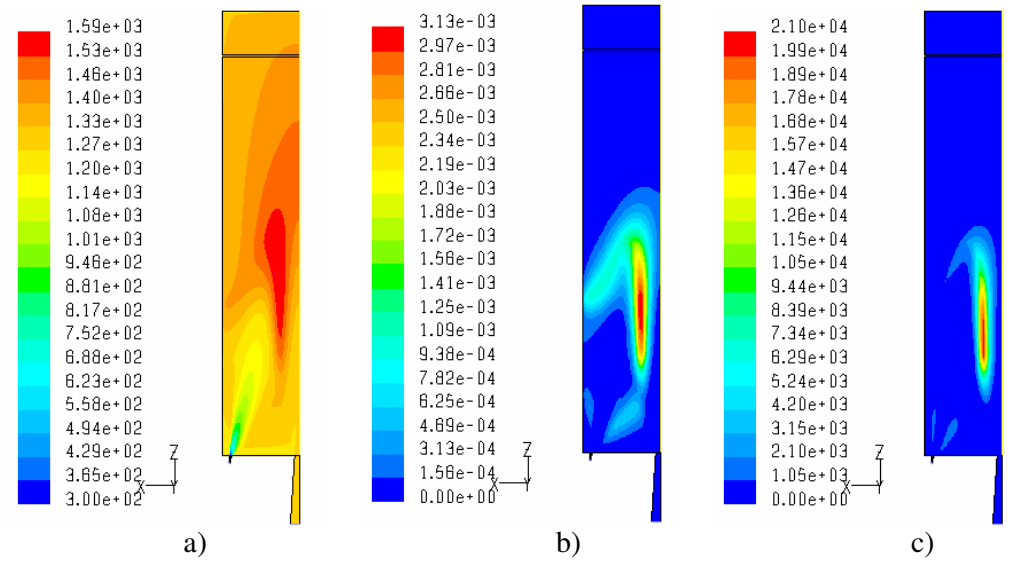

Figure 5. Simulation results: Φ_g = 30 kW - T_a= 1000 °C – E = 10% - Imm = 0.5 m a) Temperature field [K]. b) CO mole fraction field. c) Heat release field [kW/m^3].

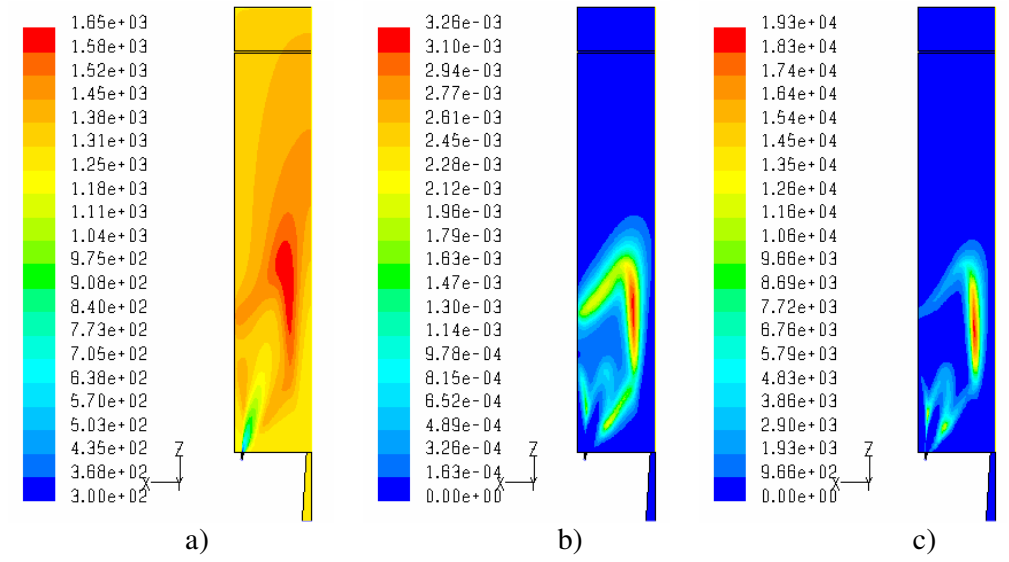

Figure 6. Simulation results: Φ_g= 30 kW - T_a= 1000 °C – E = 20% - Imm = 0.5 m a) Temperature field [K]. b) CO mole fraction field. c) Heat release field [kW/m^3].

In the following, the first regime will be designated as "near-lifted flame" and the second one as "far-lifted flame", as in Lille et al. (2005).

The reaction zone prediction is validated by comparing measured OH emission and computed heat release, with reference to the work by Hardalupas and Orain (2004), who consider the OH radical intensity a good marker of the rate of heat release. Due to the "line-of-sight" nature of the OH images, computed values have to be integrated along the furnace width to be comparable with experimental profiles.

The integrals of specific heat release computed in

planes perpendicular to the vertical axis (Z-plane) are plotted in Figure 9; they are consistent with the corresponding OH emission profiles extracted from the recorded images (Figure 3).

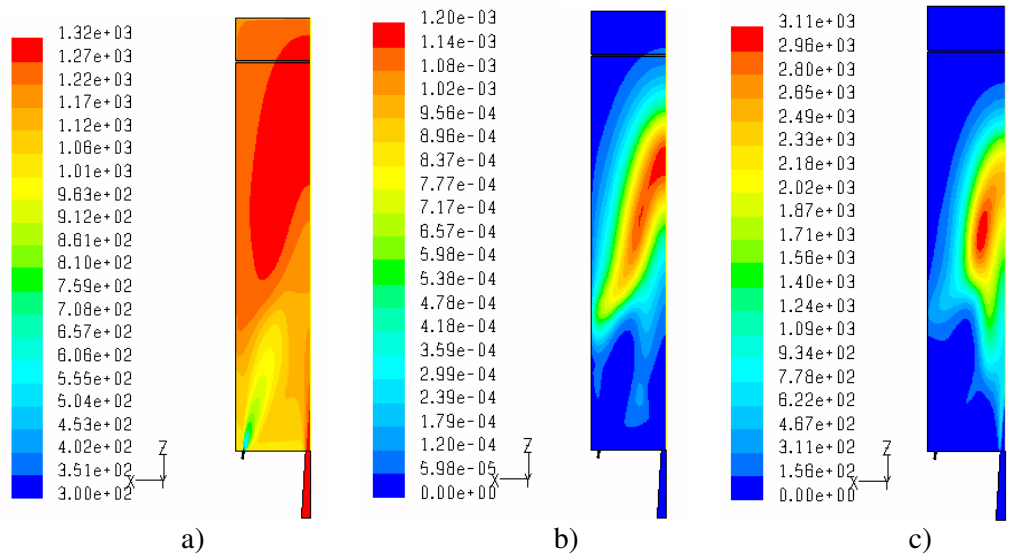

Figure 7. Simulation results: Φ_g= 30 kW - T_a= 1000 °C – E = 10% - Imm = 0.7 m a) Temperature field [K]. b) CO mole fraction field. c) Heat release field [kW/m^3].

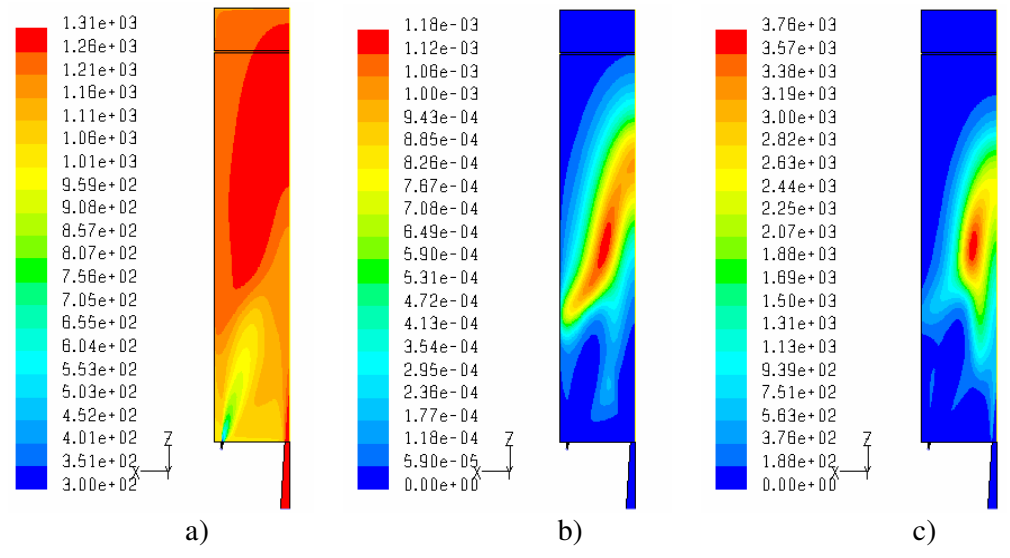

Figure 8. Simulation results: Φ_g= 30 kW - T_a= 1000 °C – E = 20% - Imm = 0.7 m a) Temperature field [K]. b) CO mole fraction field. c) Heat release field [kW/m^3].

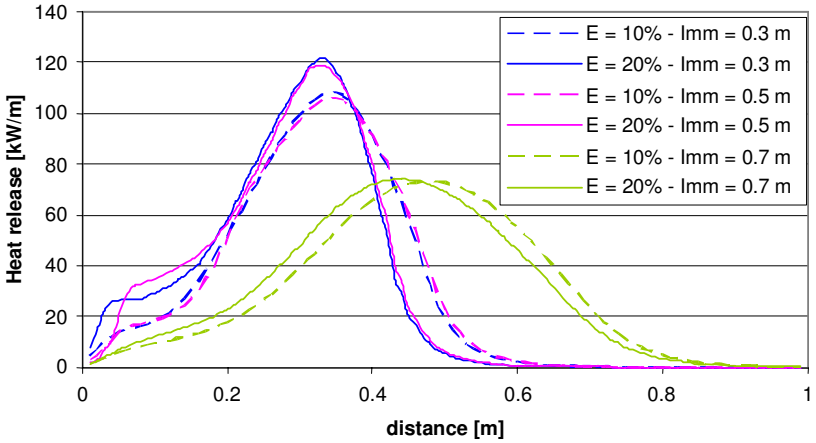

Figure 9. Simulated heat release evolution.

Figures 3 and 9 show that the "near-lifted flame" regime occurs when furnace temperature is high (i.e. with the lower immersion depths of the cooling tubes), regardless of the quantity of excess air.

This corresponds to OH emission profiles measured when $T_f > 1150$ °C (0.3 m immersion depth) (Figure 3) and to heat release profiles computed with $T_f > 1050$ °C (0.3 and 0.5 m immersion) (Figure 9). It is characterised by higher combustion intensity than in the second regime, as shown by comparing the peak values of the blue ("near-lifted") and orange ("far-lifted") OH intensity curves (Figure 3). The higher combustion intensity of the "near-lifted flame" regime is reproduced by the computed heat release profiles (Figure 9). Figures 3 and 9 also show that the intensity of the "near-lifted flame" combustion regime increases slightly with increasing excess air, but that the peak location, between 0.30 and 0.35 m from the furnace base, is rather insensitive to excess air conditions.

On the other hand, the "far-lifted flame" regime (Figures 7 and 8), with lower combustion intensity, occurs with the lowest furnace temperature. Figure 9 shows that this second regime is obtained when computed furnace temperature is lower than 1000 °C (immersion = 0.7 m). The peak location, also independent of excess air conditions, is in that case between 0.45 and 0.5 m from the furnace base. Due to safety constraints on the experimental set-up (safety of temperature at furnace base imposed above 800 °C to ensure gases flammability), such low furnace outlet temperatures are not measurable.

Transition between these 2 regimes may occur at intermediate furnace temperatures, depending on the excess air conditions. The cyan and orange curves in Figure 3 show that, at around 1100 °C furnace outlet temperature (measured here with 0.6 m immersion depth of the tubes), a lower excess air leads to the "far-lifted flame" regime, while combustion is near the furnace base when E = 20%. In the latter case, the higher oxygen content of the recirculated flue gases increases the reaction rates near the injection zone, and the higher inlet air flow rate increases the air jet momentum; this could enhance the air jet entrainment and could result in a higher mixing intensity than with lower excess air.

The recirculation ratio, computed in the Z-planes as the ratio of the mass flow rate flowing in the negative Z direction to the total inlet mass flow rate, is quasi-independent of excess air settings, as seen in Figure 10. One can also observe in Figure 10, that the maximum recirculation ratio is higher than 5, as it is recommended in Hasegawa and Tanaka (1998) for flameless oxidation and that the profiles are not very dependent on furnace temperature.

The flame regime computed by the CFD model is always independent of excess air. This could indicate that none of the modelled cases is in the intermediate region of furnace temperature. Further investigation is needed, namely by adjusting the model heat losses to be able to correctly and accurately predict the furnace temperature in the vicinity of the transition region.

Furnace wall temperature profiles

The evolution of temperatures computed at the furnace wall is plotted in Figure 11. The profiles corresponding to the higher furnace temperature, i.e. to the "near-lifted flame" regime, and exhibit a peak at 0.32 m from the furnace base, while no peak can

be observed with the "far-lifted flame" regime. The peak value is higher for higher excess air. This can be interpreted as the effect of the secondary combustion zone, which occurs near the furnace wall due to combustion of the gas jet meeting the residual oxygen contained in the recirculating gases. In that case, the higher residual oxygen in the flue gases, with higher excess air, causes a higher heat release near the wall and, therefore, a higher wall temperature (Figure 11).

However, the measured wall temperatures do not show the peak values of the computed corresponding profiles, which seems to indicate that the secondary combustion zone is not always present near the wall. Unfortunately, the secondary reaction zone is not visually accessible to the CCD intensified camera and that assumption has, therefore, not been validated.

Conclusions and Perspectives

In the present study, a CFD model of flameless combustion in a laboratory scale furnace was developed to investigate the influence of the furnace temperature and excess air ratio on the combustion zone. The model has been validated against measured values of OH emission intensity and furnace wall temperature profiles.

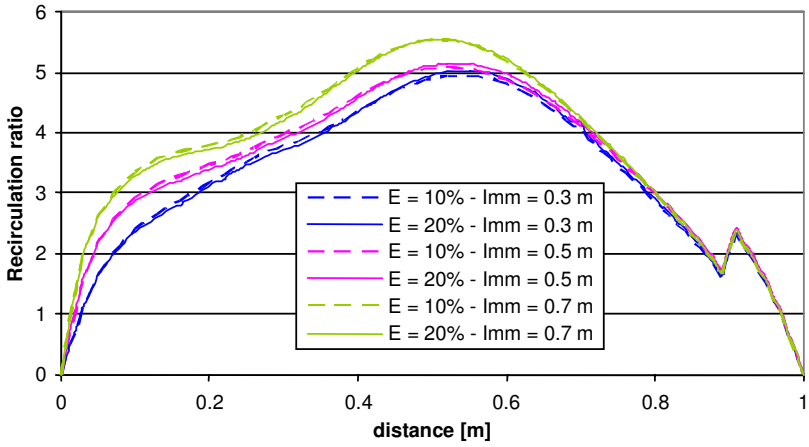

Figure 10. Simulated recirculation ratio evolution.

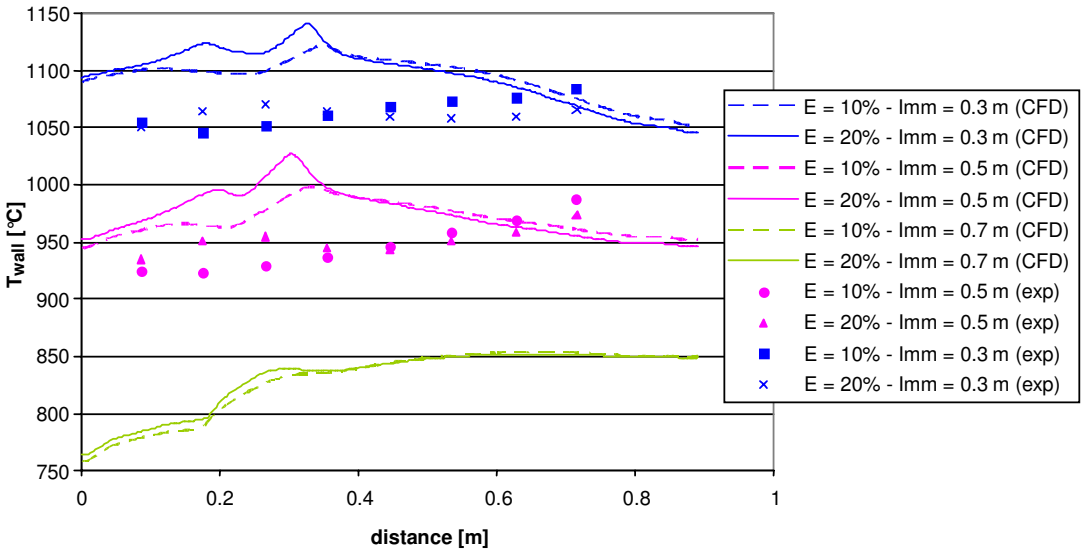

Figure 11. Simulated wall temperature evolution.

Two significantly distinct combustion regimes have been observed in the simulation. The "near-lifted flame" regime develops when furnace temperature is high and is characterised by 2 separate and intense reaction zones that are symmetrical with respect to the furnace axis. In this regime, a secondary combustion zone is predicted in the recirculating flow and its intensity depends on the residual oxygen content in the flue gases.

The "far-lifted flame" regime occurs when furnace temperature is lower. In that lower-temperature condition, the reaction rates decrease and, therefore, probably become controlled more by kinetic limitation than by mixing velocity. The reaction zone is wider than in the first regime and located farther downstream of the injectors.

The primary reaction zone prediction is fairly well validated by the measured OH emission profiles, except in intermediate furnace temperature conditions (when outlet gases temperature (T_f) is around 1100 °C), when the measured reaction zone location depends on excess air, whereas the predicted one does not.

These discrepancies indicate that the agreement of the computed and measured furnace outlet temperatures should be better than 50 °C, which is not the case with the current model. Further modelling efforts will therefore be performed, first by adjusting the model boundary conditions to be able to better reproduce the various terms of the furnace heat balance, and consequently to predict more correctly and precisely the furnace temperature in the vicinity of the transition region.

Furthermore, the secondary reaction zone is not visually accessible to the CCD intensified camera and has, therefore, not been validated. To obtain additional information, further experimental investigations are planned, with in-furnace local temperature and species measurements. Laser velocity measurements will also be performed to characterise the evolution of the in-furnace recirculation ratio.

Acknowledgements

This work has been performed within the framework of a research programme funded by the Walloon Government. The authors wish to thank the Walloon regional authorities for their financial support.

Nomenclature

E	excess air ratio
Imm	immersion depth of the cooling tubes (m)
T_a	air temperature (°C)
T_f	flue gases temperature (°C)
Φ_g	fuel heat rate (kW)
ε	emissivity

References

Hardalupas, Y. and Orain, M., "Local measurements of the time-dependant heat release rate and equivalence ratio using chemiluminsecent emission from a flame", Combustion and Flame, 139, 188-207, 2004.

Hasegawa, T. and Tanaka, R., "High Temperature Air Combustion - Revolution in Combustion Technology - (Part I: New Findings on High Temperature Air Combustion)", JSME International Journal, Series B, 40, 1079-1084, 1998.

Lille, S., Blasiak, W. and Jewartowski, M., "Experimental Study of the Fuel Jet Combustion in High Temperature and Low Oxygen Content Exhaust Gases", Energy, 30, 373-384, 2005.

Murer, S., Pesenti, B. and Lybaert, P., "Characterization of Flameless Combustion of Natural Gas in a Laboratory Scale Furnace", Proceedings of the European Combustion Meeting 2005, Louvain-La-Neuve, Belgium, April 2005.

Westbrook, C. and Dryer, F., "Simplified Reaction Mechanisms for the Oxidation of Hydrocarbon Fuels in Flames", Combustion Science and Technology, 27, 31-43, 1981.

Wünning, J.A. and Wünning, J.G., "Flameless Oxidation to Reduce Thermal NO-Formation", Progress in Energy and Combustion Science, 23, 81-94, 1997.